ResearchGate

See discussions, stats, and author profiles for this publication at: https://www.researchgate.net/publication/255749526

Hydrothermally highly stable acidic mesoporous aluminosilicate spheres with radial channels

ARTICLE *in* JOURNAL OF MATERIALS CHEMISTRY · DECEMBER 2010

Impact Factor: 7.44 · DOI: 10.1039/C0JM01973A

CITATIONS
6

READS
11

9 AUTHORS, INCLUDING:

Xiaohui Liu
East China University of Science and Techn…
80 PUBLICATIONS **1,387** CITATIONS
SEE PROFILE

Jiawen Ren
George Washington University
55 PUBLICATIONS **1,731** CITATIONS
SEE PROFILE

Yanqin Wang
East China University of Science and Techn…
708 PUBLICATIONS **14,206** CITATIONS
SEE PROFILE

Wolfgang Schmidt
Max Planck Institute for Coal Research
125 PUBLICATIONS **3,928** CITATIONS
SEE PROFILE

Available from: Yanqin Wang
Retrieved on: 24 January 2016

Hydrothermally highly stable acidic mesoporous aluminosilicate spheres with radial channels†

Xin Gu,[a] Tianlong Jiang,[a] Haixiang Tao,[a] Shutian Zhou,[b] Xiaohui Liu,[a] Jiawen Ren,[a] Yanqin Wang,*[a] Guanzhong Lu[a] and Wolfgang Schmidt*[b]

Received 22nd June 2010, Accepted 27th September 2010
DOI: 10.1039/c0jm01973a

Hydrothermally highly stable mesoporous aluminosilicate spheres with radial channels were synthesized in the CTAB–NaF–TPAOH system through a one-step procedure at high aging temperature. The characterization by transmission electron microscopy (TEM), X-ray diffraction (XRD), nitrogen adsorption/desorption analysis, ^{27}Al MAS solid state NMR spectroscopy, pyridine adsorption FT-IR combined with the typical hydrothermal treatments showed that this kind of material exhibited large surface area, specific pore arrangement, strong acidity and high hydrothermal stability. Detailed studies suggest that F^- ions direct the perpendicular arrangement of aluminosilicate clusters during the hydrothermal treatment at 160 °C, while TPA^+ stabilized the structure. Both F^- and TPA^+ ions are considered to improve the acidity and hydrothermal stability of this material through coordination of framework atoms, thus, enhancing the condensation of Si–O–Si bonds in the amorphous pore walls. Due to the accessible radial pore arrangement and high acidity, the catalytic activity for Friedel–Crafts alkylation of toluene with benzyl alcohol was excellent with 100% conversion of benzyl alcohol.

Introduction

Solid acid catalysts, such as zeolites,[1] ion-exchanged resins,[2] sulfated zirconia,[3] and niobium phosphate,[4] have been widely investigated because of their easy separation without acid waste, high thermal/hydrothermal stability, tunable acidity and excellent selectivity towards specific products. Among those acidic catalysts, protonated zeolites are specifically favoured because of their high acidity and excellent hydrothermal stability. However, mass transfer limitation of bulky molecules often hampers the use of microporous zeolites as catalysts for the synthesis of pharmaceutical, biological, and fine chemicals. Since the catalytic reaction rate and selectivity are sensitive to transport restrictions, aluminium-containing mesoporous materials have been used for reactions of larger molecules.[5–10]

Mesoporous materials with large pore sizes and different pore arrangements could improve the catalytic activity or change product distributions. However, usually the amorphous pore walls can not resist severe hydrothermal conditions, such as often used for catalytic reactions. Therefore, substantial research has been focused on improving the hydrothermal stability of mesoporous materials, *e.g.*, using triblock copolymer as template to synthesize materials with thicker pore walls,[11] removing silanol groups by silylation,[12] taking advantage of salt effects,[13,14] using a co-templating approach,[15,16] or post-synthetic treatments.[17] Xia reports that the resistance of fluorinated surfaces against hydrolysis by water molecules is remarkably improved, resulting in hydrothermal stability of the mesopore framework.[18] Using fluoride anions or fluoride salts as additives often results in hydrothermally highly stable silicate mesostructures. Chen and co-workers reported that using nonionic organosilicon surfactant as template and sodium fluoride as additive, highly stable mesoporous silica can be synthesized.[19] These surveys confirmed the advantages of using fluoride salts as additives for improving hydrothermal stability of amorphous silicate frameworks. Addition of fluoride ions could also enhance the acidity by coordinating the silicon atoms and thus modifying Brønsted and Lewis acidity at the surface of aluminosilicate materials.[20,21] Aluminium substitution of silicon in silicates can generate acidic sites. With controlled fluoride addition, aluminium-substituted mesoporous SBA-15 (Al-SBA-15) materials can be directly synthesized.[22] Moreover, taking advantage of both high acidity and excellent hydrothermal stability of zeolites, mesoporous materials with semi-crystallized pore wall could be obtained using primary and secondary zeolite nanoclusters as building units.[23–26]

For mesoporous materials, the variability of their pore structures and their potential for diverse applications are driving forces for research. Among the possible pore arrangements, radially aligned mesopores should be well accessible. A "modified Stöber method"[27] was used to synthesize silica with such radially oriented mesopores. Using ethanol as both template and co-solvent, the CTAB-templated mesopore morphology could be transferred to radial pores in the TEOS-CTAB-water-tetraalkyl ammonium system.[28] In the highly concentrated ethanol solution, TEOS hydrolysis is a rather slow process facilitating alignment of micelles extending from the center of the spheres.[29]

[a]*Key Lab for Advanced Materials, Research Institute of Industrial Catalysis, East China University of Science and Technology, Shanghai, 200237, P. R. China. E-mail: wangyanqin@ecust.edu.cn; Fax: +86 21 6425 3824; Tel: +86 21 6425*
[b]*Max-Planck-Institut für Kohlenforschung, Kaiser-Wilhelm-Platz 1, 45470 Mülheim an der Ruhr, Germany. E-mail: schmidt@mpi-muelheim.mpg.de; Fax: +49 208 306 2995; Tel: +49 208 306 2370*

† Electronic supplementary information (ESI) available: Wide angle XRD pattern, t-plot and sketch of subdomains with radially arranged mesopore channels. See DOI: 10.1039/c0jm01973a

 This journal is © The Royal Society of Chemistry 2011

TEM images and small angle electron diffraction (ED) patterns verified the radial arrangement of mainly cylindrical pores.[30] In previous reports, formation of mesoporous silica with radial channel structures was reported to be possible with anionic[31,32] or fluorocarbon surfactants[33] in ethanol-free solutions. Also surface-functionalized silicate particles with radially arranged pore arrangement have been reported.[32] Because of the unique pore systems, applications in drug delivery as well as in catalysis were the focus of the authors. Recently, we discovered an alternative method for the synthesis of mesoporous aluminosilicate with radially oriented pores, applying hydrothermal reaction conditions similar to those applied in zeolite synthesis. The acidity and hydrothermal stability of the obtained material exceeded those of previously reported ones.

In this paper we describe a simple one-pot reaction that allows the direct synthesis of such materials using a combination of fluoride (NaF) and tetrapropylammonium hydroxide (TPAOH) as additives. Characterization of the solids by TEM, XRD, N_2 sorption analysis, ^{27}Al MAS solid state NMR, and NH_3-TPD proved the existence of a radial pore arrangement, relatively high acidity, high specific surface areas (around 800 m^2g^{-1}), and high pore volumes (up to 0.75 cm^3g^{-1}). Their mesopore structures and surface areas were well maintained upon boiling the materials in water or treatment with water vapor at 600 °C. The influences of F^- ions and TPAOH on the formation of the radial pore structure and acidity were investigated in detail. Alkylation of toluene with benzyl alcohol was used to evaluate the catalytic performance of the obtained materials.

Experimental

Chemicals

Sodium fluoride (NaF), cetyltrimethylammonium bromide (CTAB), tetraethyl orthosilicate (TEOS) and tetrapropylammonium hydroxide (TPAOH) were purchased from Shanghai Chemical Co. All chemicals were used without further purification.

Synthesis

In a typical synthesis, 0.01 g NaF, 0.2 g CTAB and 3.2 ml TPAOH (25 wt%) were dissolved in 96 g de-ionized water at 35 °C in a water bath. The mixture was stirred until it became transparent. Then, 1.1 g TEOS was dropped into the homogeneous solution under vigorous stirring that was continued for 30 min. Then, the calculated amount of $NaAlO_2$ (the molar ratio of silicon to aluminium was 30 : 100) was added to the solution. After stirring for another 30 min, the resulted suspension was aged at 160 °C for 3 days. The white precipitate was filtered, washed with de-ionized water and dried at 60 °C over night. Finally, the powder was calcined in air at 550 °C for 5 h to completely remove the organic surfactants. The samples after calcination were denoted as $SiAl_X$-Y-Z, in which X is the molar ratio of silicon to aluminium, Y the aging temperature, and Z the aging time. For example, $SiAl_{50}$-160-3 is a sample with Si/Al = 50 that was aged at 160 °C for 3 days. For comparison, samples that were synthesized without NaF or TPAOH or neither of these two compounds (aging at 160 °C for 3 days) were denoted as $SiAl_{50}$-160-3-T, $SiAl_{50}$-160-3-F and $SiAl_{50}$-160-3-N, respectively.

Hydrothermal stability

The hydrothermal stability was tested by treating the samples in boiling water for 5 days. The samples have been denoted as $SiAl_X$-Y-Z-B. Those that have been treated in water vapor at 600 °C for 4 h were denoted as $SiAl_X$-Y-Z-V.

Alkylation

The liquid phase benzylation of toluene with benzyl alcohol was carried out in a three-necked round-bottom flask equipped with a reflux condenser, heated in a temperature-controlled oil bath (110 or 140 °C) under atmospheric pressure. In a typical run, 0.05 g catalyst was added to the mixture of 1.8 g toluene and 0.54 g benzyl alcohol. The molecular ratio between reactants in solution and Al in catalyst was 1 toluene : 0.25 benzyl alcohol : 1.7×10^{-3} Al for sample $SiAl_{50}$-160-3. The moment of addition of the catalyst was taken as reaction time zero. Liquid samples were withdrawn by centrifugation after reacting for 2 h. They were analyzed on a Perkin Elmer Clarus 500 gas chromatograph with a HP5 column and a FID detector. The products were identified by GC-MS analysis. The conversion was calculated based on benzyl alcohol.

Characterizations

X-Ray diffraction (XRD) patterns were recorded on a Rigaku D/max-2550VB/PC diffractomer using Cu-Kα radiation (λ = 1.5418 Å). Fourier Transform Infrared (FT-IR) spectra were measured on a Nicolet 710 spectrometer using KBr pellets. Nitrogen physisorption isotherms were measured at 77 K with a Quantachrome Nova 4200e sorption analyzer. NLDFT pore size distributions were calculated from the adsorption and desorption branch using models for nitrogen adsorption at 77 K on silica with cylinder pores. The total pore volume is calculated at the point of $p/p_0 = 0.99$. Before the measurement, the samples were outgassed at 473 K for 10 h. Transmission Electron Microscope (TEM) images were obtained with a FEI Tecnai 20 S-TWIN instrument operated at 200 kV. ^{27}Al MAS solid state NMR spectra were recorded at a frequency of 130 MHz on a Bruker DRX-500 spectrometer equipped with a 4mm MAS BB-1H probe at room temperature, NH_3-TPD experiments were carried out on a PX200 instrument from Tianjin Golden Eagle Technology Co. LTD. Prior to the measurements, about 80 mg of sample were activated by heating at 773 K for 2 h, and after cooling to 293 K, ammonia adsorption was carried out at 323 K for 45 min. Physically adsorbed ammonia was removed by purging with nitrogen at 363 K for 2h. NH_3-TPD experiments were carried out by increasing the cell temperature linearly from 363 to 1123 K with a heating rate of 10 K min^{-1} and a helium flow rate of 35 cm^3 min^{-1}.

Results and discussion

Fig. 1 shows SEM and TEM photographs of the as-synthesized silica-alumina material, $SiAl_{50}$-160-3, with and without aging under synthesis conditions. The SEM photographs of the materials obtained without aging shows particles with a rather uniform particle size of 2 μm (Fig. 1a). Tan *et al.*[34] reported the formation of spherical silica particles with radially oriented

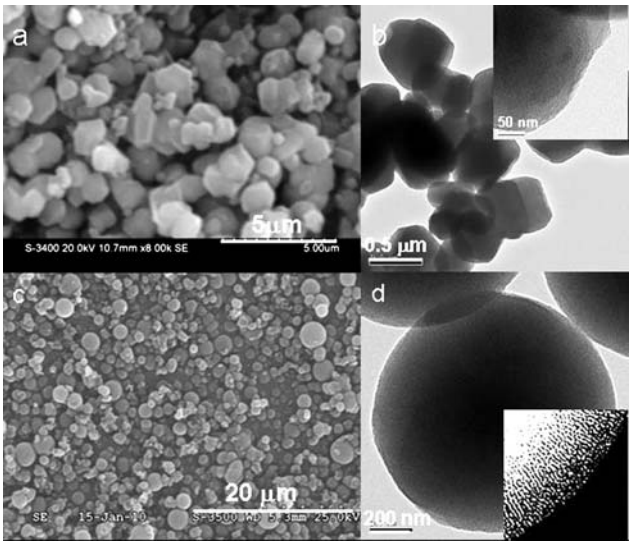

Fig. 1 SEM and TEM images of sample $SiAl_{50}$-160-3 before (a, b) and after aging process (c, d).

mesopores in a solution of ethanol, water and ammonia using a cationic surfactant. Weakly connected disordered clusters have been supposed to associate as larger spherical aggregates exposing radially oriented mesopores. From the high resolution TEM (Fig. 1b), no obvious radial channel structure was observed in our sample as shown in the inset. After aging at 160 °C for 3 days, a notably different morphology (Fig. 1c) and channel orientation was observed, as shown in Fig. 1d. The shape of the particle transformed to spheres probably as the result of minimization of free energy of surface[35] and the size of the particles increased to 2–5 μm. About 30% of crushed particles have been observed in the SEM images. However, crystalline ZSM-5 zeolite particles, that could have resulted from the use of TPA^+ as template, have been not observed. Only amorphous silica was detected by wide-angle X-ray diffraction (shown in Figure S1†) indicating that no larger ZSM-5 particles formed. This might be attributed to the high pH value (pH = 12) which is somewhat higher than in typical reaction mixtures for ZSM-5 crystallization. The SEM images also confirmed the absence of larger crystalline particles. The high resolution TEM image shows that the channels of these 0.5–2 μm spheres extend perpendicular to the outer surface. The mesopore wall thickness is uniform in the range of 1–2 nm and the pore size is in the range of 3–4 nm, which agrees with the textural properties of typical CTAB-templated materials. Although some twisted disordered regions are occasionally observed, especially in the center, all channels seem to start from the center and extend to the surfaces of the spheres as indicated by the image after adjusting the contrast threshold (ImageJ software package) in Fig. 1d (inset). The aging process seems to play an important role in the formation of radial orientation of the pores, and slow silica vitrification at high pH is probably favourable for this orientation.[34]

Fig. 2 shows the low angle X-ray diffraction pattern and N_2 physisorption for sampe $SiAl_{50}$-160-3. The broad peaks in the low angle XRD pattern in Fig. 2(a) indicated a less ordered structure. However, broad reflections are visible at positions that are indicative of a hexagonal pore arrangement ((100), (110), and

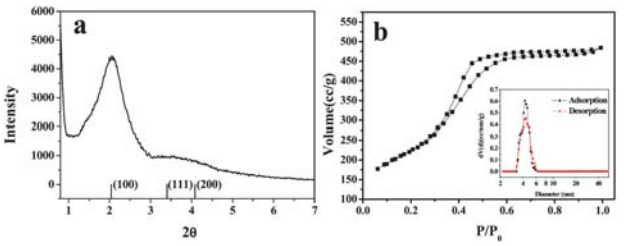

Fig. 2 Low angle XRD pattern (a), nitrogen-sorption isotherm (b) and NLDFT pore size distribution (inset) of sample $SiAl_{50}$-160-3.

(200) reflections). N_2 physisorption was used to investigate the sorptive properties of the materials, *i.e.*, specific surface area, pore size, and pore volume. Fig. 2 (b) shows the N_2 sorption isotherm of sample $SiAl_{50}$-160-3, which is a typical type IV isotherm with H1 hysteresis loop. The uptake at a relative pressure of $p/p_0 = 0.3 \sim 0.5$ is characteristic for capillary condensation in mesopores. The pore size distribution indicates rather uniform mesopore diameters. The specific surface area (B.E.T.) and total pore volume ($p/p_0 = 0.99$) are 798 $m^2\ g^{-1}$ and 0.75 $cm^3\ g^{-1}$, respectively, while no micropores were detected (verified by t-plot as shown in Figure S2†). NLDFT evaluation of the adsorption branch of sample $SiAl_{50}$-160-3 shows a distinguished maximum of the pore size distribution at about 4.2 nm and a slightly broader maximum at 4.4 nm that was calculated from the desorption branch. The delay of desorption at pressures below $p/p_0 = 0.42$ could be the result of textural porosity of aggregated silica sub-particles in the spheres. The spheres must consist of sub-domains since not all pores of uniform size can extend to the center of the spheres, simply for steric reasons. Between the sub-domains larger pores can be envisaged that are accessible only *via* very long mesopores of the sub-domains. In such voids N_2 molecules may get trapped during desorption (schematically shown in Figure S3†). As the result, desorption from these pores is delayed since it can only occur after the extended mesopores of the subdomains have been emptied.

The amount of aluminium in the framework as well as its coordination determines the acidity of silicates. In order to investigate the acidic properties of the obtained materials, several methods have been used. The amounts of the elements Al and Si of $SiAl_{0.5}$-160-3 were measured using ICP-AES. The Si/Al molar ratio was 47, close to the composition in the initial gel (Si/Al = 50). Nearly all aluminium remained in the final material after aging for 3 days. ^{27}Al-MAS NMR spectra allowed identification of the coordination state of aluminium in the silicate framework (Fig. 3). The band at 54 ppm corresponds to tetrahedrally coordinated Al and the broad band at 0 ppm is ascribed to the octahedrally coordinated Al. The tetrahedrally coordinated and the octahedrally coordinated aluminium species were associated with Brønsted acid sites and Lewis acid sites, respectively. The IR spectrum of pyridine in Fig. 4 confirms that both types of acid sites exist in sample $SiAl_{50}$-160-3. The band at 1453 cm^{-1} is characteristic of pyridine interacting with Lewis acid sites, whereas that at 1542 cm^{-1} corresponds to the Brønsted acid sites, the one at 1490 cm^{-1} is assigned to both sites.[36]

The acid strength was investigated by temperature programmed ammonia desorption (NH_3-TPD), as shown in Fig. 5. The low temperature (LT) peak at around 210 °C is due to weak

 This journal is © The Royal Society of Chemistry 2011

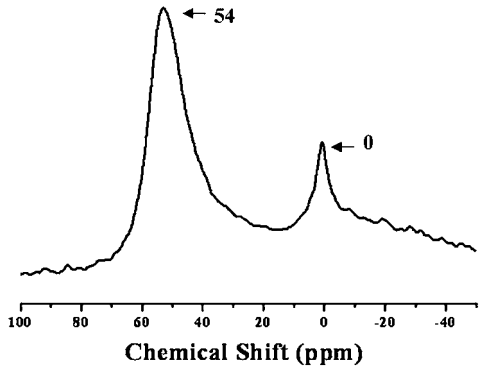

Fig. 3 ^{27}Al solid state NMR spectrum of sample $SiAl_{50}$-160-3.

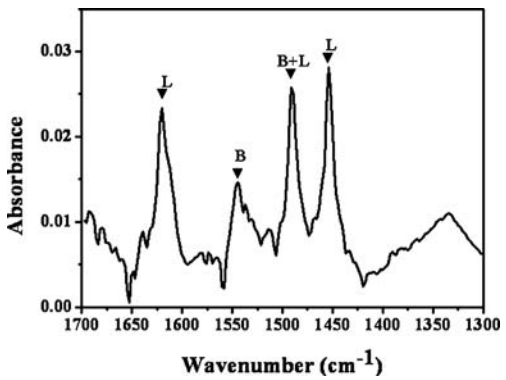

Fig. 4 IR spectrum of pyridine adsorbed on sample $SiAl_{50}$-160-3. The sample was activated at 150 °C before exposure to pyridine and evacuated at 200 °C.

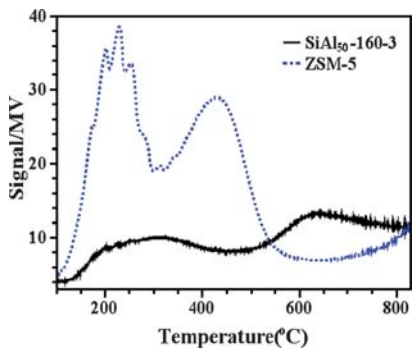

Fig. 5 NH_3-TPD curves obtained on sample $SiAl_{50}$-160-3 and commercial ZSM-5 (Si/Al = 50) after evacuating the NH_3-loaded sample at 363 K for 2 h. About 80 mg sample was heated in He flow at a rate of 10 K min^{-1}.

acid sites. The high temperature (HT) peak, appearing above 300 °C, corresponds to ammonia desorbing from strong acid sites with Hammett acidity function $H_0 \leq -3$.[37] Although the amount of ammonia desorbing from sample $SiAl_{50}$-160-3 is less than that from the ZSM-5 (Si/Al = 50), it is interesting that the HT peak is observed at around 650 °C for $SiAl_{50}$-160-3, indicating the existence of rather strong acid sites. This could be attributed to the complexity of the silica-alumina wall in which the chemical environment of both Al and Si were greatly influenced by the synthesis method. As Le Van Mao and coworkers[38] reported, small amounts of F^- in this system could partly coordinate OH bridges and enhance the acidity of the remaining SiOH groups. In addition, the presence of Al–F species could increase the acidity by increasing the acid strength of the framework species.[36] As Hunger showed by ^{19}F-NMR,[39] treatment of (Al)MCM-41 with ammonium fluoride not only results in the formation of F–Si species but also some hexagonally coordinated fluoride aluminium species, $^{VI}Al(O_5F)$, are generated. Thus, the existence of octahedrally coordinated aluminium, as shown in the ^{27}Al-MAS NMR spectra (Fig. 3, signal at 0 ppm), could be partly due to the formation of aluminium species coordinated by F^-.

In conclusion, the obtained aluminosilicate material with radially oriented pores should provide active sites for acid catalysis due to acidic aluminium sites in the framework, either exposed to the surface or the pore channels.

To prove the hypothesis that F^- ions and TPA^+ affected the pore arrangement, three samples either without NaF, TPAOH, or both of them were synthesized and denoted as $SiAl_{50}$-160-3-T, $SiAl_{50}$-160-3-F and $SiAl_{50}$-160-3-N, respectively. All the samples were synthesized according to the same synthesis protocol as sample $SiAl_{50}$-160-3. As shown in Fig. 6, no radial channels are visible for sample $SiAl_{50}$-160-3-N but only small particles (100–150 nm) with worm-like pore structure (NaOH used as base instead of TPAOH, pH = 12). For sample $SiAl_{50}$-160-3-F, a fraction of small spheres showed radially oriented mesopores and the rest had worm-like pore arrangement. Sample $SiAl_{50}$-160-3-T was totally different, large fiber-like particles were observed, and no spherical particles were formed. Thus, TPA^+ ($SiAl_{50}$-160-3-T) seems to be not responsible for the formation of radially arranged pores, but it seems to enhance the thermal stability of the mesoporous framework.[40] Compared with sample $SiAl_{50}$-160-3-T, the small mesoporous spheres with radially arranged channels in sample $SiAl_{50}$-160-3-F indicate that the unique radial arrangement of pores is probably induced by the interaction of fluoride anions with the silica. The F^- ions not only facilitated the hydrolysis of silicate precursor but also directed the channels alignment perpendicular to the extra-surface of the particle during the hydrothermal high temperature treatment.

Both F^- ions and TPA^+ took part in the formation of the radially arranged mesopores in the spheres. However, not only the morphology but also the acidity was improved with the addition of F^- and TPA^+. The F^- ions seemed to improve the acidity by coordinating silicon or aluminium in the framework as discussed above. About the role of the TPA^+, which is usually

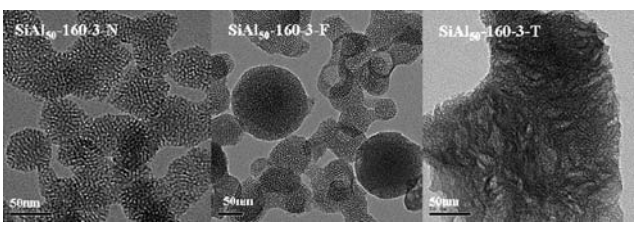

Fig. 6 TEM images of sample $SiAl_{50}$-160-3-N obtained without addition of NaF and TPAOH, $SiAl_{50}$-160-3-F without addition of TPAOH and $SiAl_{50}$-160-3-T without addition of NaF.

used to direct crystallization towards MFI-type zeolites (ZSM-5), one could only speculate. It might be responsible for the formation of tiny aluminosilicate clusters with tetrahedrally coordinated aluminium, such as found in zeolites. The as-synthesized materials thus combine the advantages of zeolite-like aluminium coordination, resulting in high acidity, and high hydrothermal stability. Although wide angle XRD patterns showed the existence of only amorphous aluminosilicate for all the samples, IR spectra reveal specific properties of the pore walls of the materials.[41] For a typical IR spectrum of zeolites, the absorption 550–420 cm^{-1} is assigned to the internal vibrations of the SiO_4 and AlO_4 tetrahedra that are also observed in silica or quartz. Bands in the range of 650–500 cm^{-1} are assigned to the presence of double-rings of tetrahedra that usually do not exist in pure silica.[42,43] Hence, the ratio between the bands at 650–500 cm^{-1} and 550–420 cm^{-1} might be an indication for the existence of zeolite-like sub-structures.[41] The FT-IR spectra in Fig. 7 show that the intensity ratio of the absorption bands at 550 cm^{-1} and 450 cm^{-1} is larger for sample $SiAl_{50}$-160-3-T than for the samples $SiAl_{50}$-160-3-F and $SiAl_{50}$-160-3-N. The latter showed almost no absorbance at around 550 cm^{-1}, and the slightly higher intensity ratio of sample $SiAl_{50}$-160-3 could be attributed to the improvement of the condensation of the silicate due to the addition of F^- ions. Thus, the high acidity and hydrothermal stability of the mesoporous aluminosilicate framework could be partly attributed to contributions of TPA^+, *i.e.*, increasing the number of zeolite-like aluminium sites and the interaction of F- with both silicon and aluminium. The specific surface areas and pore volumes of $SiAl_{50}$-160-3-N, $SiAl_{50}$-160-3-F, and $SiAl_{50}$-160-3-T were 556, 668, 717 m^2g^{-1} and 0.57, 0.68, 0.63 cm^3g^{-1}, respectively. All these samples had lower surface areas than sample $SiAl_{50}$-160-3.

The hydrothermal stability was studied by treating samples in boiling water for 5 days or with water vapor at 600 °C for 4 h (denoted as $SiAl_{50}$-160-3-B and $SiAl_{50}$-160-3-V). Fig. 8 and 9 show the TEM images and N_2 sorption isotherms of sample $SiAl_{50}$-160-3 after the hydrothermal treatments. The TEM images show that the radial channels are maintained with only minute structural collapse. As shown in Fig. 9, the hysteresis loop of N_2 physisorption becomes broader for sample $SiAl_{50}$-160-3-V, which suggested certain leaching of silicate from the pore structure and formation of larger pores. The even more broadened hysteresis loop of sample $SiAl_{50}$-160-3-B indicated a somewhat more severe dissolution and rearrangement of silica and the generation of different-sized pores. Only 3% and 8% of the specific surface area were lost during treatment with water vapor and boiling water. The materials thus has a remarkable stability at high temperatures and hydrothermal treatment.

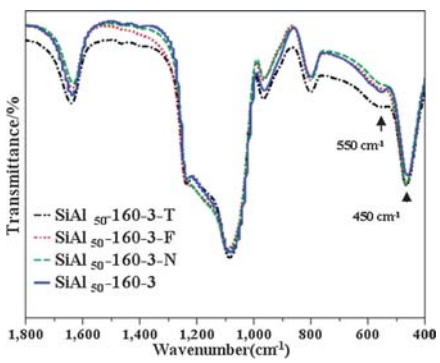

Fig. 7 IR spectra of samples $SiAl_{50}$-160-3-N, $SiAl_{50}$-160-3-F, $SiAl_{50}$-160-3-T, and $SiAl_{50}$-160-3.

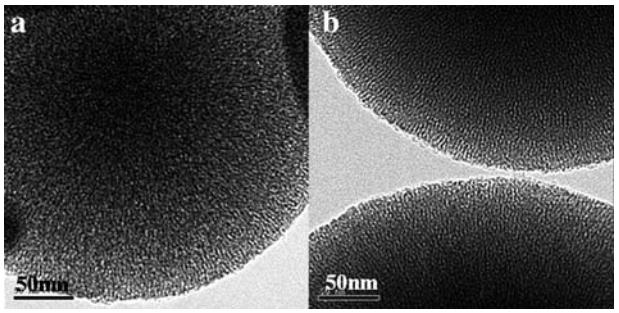

Fig. 8 TEM images of the samples (a) after boiling in water for 5 days ($SiAl_{50}$-160-3-B) and (b) after vapor treatment at 600 °C for 4 h ($SiAl_{50}$-160-3-V).

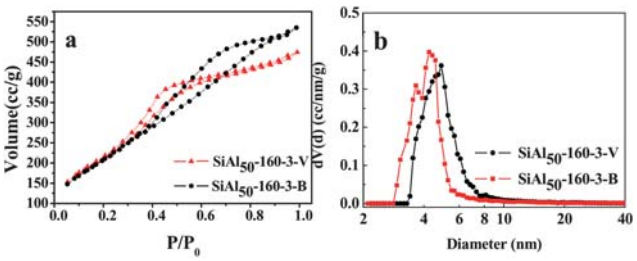

Fig. 9 (a) N_2 sorption isotherms and (b) NLDFT pore size distribution (desorption branch) of sample $SiAl_{50}$-160-3-V and sample $SiAl_{50}$-160-3-B.

The catalytic activities of the samples were investigated in the liquid phase benzylation of toluene with benzyl alcohol. From their study on diffusion effects during benzylation of toluene, Chiu and coworkers[8] concluded that mass transfer limitation partly influenced the reaction rate and product selectivity over different mesoporous and microporous materials. Therefore, ZSM-5 with a small pore size but high acidity was used as a reference for our investigations to evaluate the effect of transfer limitation on catalytic activity. Samples $SiAl_{50}$-160-3-T, $SiAl_{50}$-160-3-F, and $SiAl_{50}$-160-3-B were also used to investigate the influence of pore arrangement on the catalytic activity. Because benzylation of toluene with benzyl alcohol is promoted by Brønsted acid sites,[44] samples with different Si/Al ratios were compared to illustrate the importance of the concentration of acid sites in benzylation of toluene with benzyl alcohol. The samples $SiAl_{100}$-160-3 and $SiAl_{30}$-160-3 displayed pore arrangements comparable to those of sample $SiAl_{50}$-160-3, as observed by TEM. Table 1 lists the structural and catalytic properties of all tested materials. Scheme 1 shows the conventional reaction route for the benzylation of toluene with benzyl alcohol.

The commercial ZSM-5 showed low catalytic activity in the benzylation reaction, although it has a comparably high acidity. In contrast, sample $SiAl_{50}$-160-3 converted almost all the toluene to benzyl toluene. As assumed, diffusion and mass transport play a crucial role for this reaction. Sample $SiAl_{50}$-160-3-N converted

 This journal is © The Royal Society of Chemistry 2011

Table 1 Structural properties, conversions (C), and selectivities (S) of samples in the benzylation of toluene with benzyl alcohol

Catalysts	A_{BET}/ m^2g^{-1}	V_{total}/ cm^3g^{-1}	C_{BzOH}/ %	S_{BT}/ %	S_{BE}/ %
$SiAl_{50}$-160-3-N	556	0.57	21.5	23.2	76.8
$SiAl_{50}$-160-3-F	668	0.68	45.6	29.2	70.8
$SiAl_{50}$-160-3-T	717	0.63	99.1	42.7	57.3
$SiAl_{100}$-160-3	1012	0.87	62.8	29.8	70.2
$SiAl_{50}$-160-3	798	0.75	99.5 (100)[a]	70.8 (100)[a]	29.2 (0)[a]
$SiAl_{30}$-160-3	855	0.75	99.6	72.9	27.1
HZSM-5	310	0.18	3.7	5.4	94.6

[a] The data in brackets were obtained after reaction at 140 °C for 2 h.

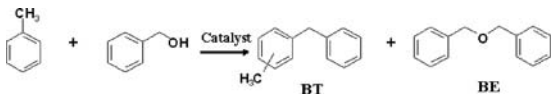

Scheme 1 Benzylation of toluene with benzyl alcohol

only 21.5% benzyl alcohol and the main product was benzyl ester (BE, by-product), which is usually catalyzed by Lewis acid sites. For sample $SiAl_{50}$-160-3-F conversion reached 45.6%, but the selectivity to benzyl toluene (BT) was only 29.2%, which was similar to sample $SiAl_{50}$-160-3-N and indicated the low acidity of these catalysts. Addition of TPA^+ caused the formation of strong acid sites in $SiAl_{50}$-160-3-T. The enhanced acidity promoted the conversion of benzyl alcohol (conversion = 99.1%). The low selectivity to BT (42.7%) may be due to different distributions of acid sites (type and strength). That is to say, the large pore size and radial pore arrangement enhance the diffusion and make the active sites accessible; the acidity enhanced by the assistance of F^- and TPA^+ resulted in higher catalytic activity.

Samples $SiAl_{50}$-160-3 and $SiAl_{30}$-160-3 showed both high benzyl alcohol conversion (more than 99%) and similar selectivity to benzyl toluene (BT) (over 70%). In contrast, sample $SiAl_{100}$-160-3 showed lower conversion of benzyl alcohol of *ca.* 62.8% with a selectivity of 29.8% to benzyl toluene (BT). This is probably attributed to a lower concentration of acid sites as the result of a lower aluminium concentration. Since all synthesized materials have high hydrothermal stability, reactions at higher temperatures were possible. As the result, 100% benzyl alcohol converted to benzyl toluene without any by-product at an increased reaction temperature of 140 °C.

Table 2 lists the properties of some catalysts as reported in literature. The catalysts had been applied in benzylation of toluene with benzyl alcohol. An as-synthesized meso/macroporous SBA-15, as obtained by Chiu and co-workers,[8] showed good activity and selectivity in Friedel–Crafts alkylation with Al/BzOH = 0.01 and toluene/BzOH = 25. In our experiments more benzyl alcohol (Al/BzOH = 0.0068 and toluene/BzOH = 4) was converted in the same period of time. This indicates that the reaction can efficiently proceed in more concentrated reaction solution with our catalysts, even at a lower Al/BzOH ratio. In the case of Al-20 SBA-15, as used in relatively concentrated reaction solution (toluene/BzOH = 9.4), less than 10% benzylalcohol was converted during the first 3 h and as long as 24 h was required to reach full conversion of benzylalcohol.[45] Because benzyl ester could also react with toluene and slowly form benzyl toluene, the 29.2% of BE could be consumed with time.[8]

Table 2 Comparison of some catalysts for the benzylation of toluene with benzyl alcohol as reported by different groups

Catalyst	Al/ BzOH	PhMe/ BzOH	*T*/ °C	t/ min	C_{BzOH}/ %	S_{BE}/ %
Al-20 SBA-15[45]	0.008	9.4	110	180	<10	30
				1440	>95	
Meso/macro-porous SBA-15[8]	0.01	25	110	100	100	7
Mesoporous SBA-15 powder[8]	0.01	25	110	100	100	21
$SiAl_{50}$-160-3	0.0068	4	110	120	99.5	29.2

Based on the catalytic performances of the aluminosilicate materials with radially oriented mesopores, the radial channels seem to facilitate mass transfer and the acidic sites exposed on the amorphous walls seem to be highly active, both factors efficiently promote the catalytic activity. The participation of F^- and TPA^+ not only affect the structural arrangement of the channels but also seem to partially modify the coordination of aluminium in the amorphous pore walls of the aluminosilicate.

Conclusion

Hydrothermally stable mesoporous aluminosilicate spheres with radial pore channels and remarkable acidity have been synthesized through the interactions between silica, CTAB micelles, fluoride anions, and TPA^+. Radial channels run perpendicular to the external surfaces of the spheres. The addition of F^- and TPA^+ was important for the final structure and acidity. The detailed formation mechanism is still unclear and further work is in progress. The synthesized aluminosilicates showed high conversion of benzyl alcohol and high selectivity to benzyl toluene in the Friedel–Crafts alkylation of toluene with benzyl alcohol. The hypothesis that fast mass transfer and accessible strong acid sites are crucial for a good catalytic performance have been verified. Combining the advantages of high hydrothermal stability, solid state acidity, and advantageous pore structure, this kind of material could be favorable also for other catalytic applications.

Acknowledgements

This project was supported financially by the 973 Program of China (2010CB732300), the National Natural Science Foundation of China (No. 20973058), the Commission of Science and Technology of Shanghai Municipality (08JC1407900, 10XD1401400) and the "Excellent scholarship" of East China University of Science and Technology, China.

Reference

1 R. J. Kalbasi, M. Ghiaci and A. R. Massah, *Appl. Catal., A*, 2009, **353**, 1–8.
2 P. R. Siril, H. E. Cross and D. R. Brown, *J. Mol. Catal. A: Chem.*, 2008, **279**, 63–68.
3 S. Ardizzone, C. L. Bianchi, G. Cappelletti, R. Annunziata, G. Cerrato, C. Morterra and P. Scardi, *Appl. Catal., A*, 2009, **360**, 137–144.
4 M. H. C. de la Cruz, J. F. C. da Silva and E. R. Lachter, *Appl. Catal., A*, 2003, **245**, 377–382.

5 Y. Yue, A. Gédéon, J. L. Bonardet, J. B. D'Espinose, J. Fraissard and N. Melosh, *Chem. Commun.*, 1999, 1967–1968.
6 A. Corma, *Chem. Rev.*, 1997, **97**, 2373–2420.
7 M. Ghiaci, H. Aghaei, M. Oroojeni, B. Aghabarari, V. Rives, M. A. Vicente, I. Sobrados and J. Sanz, *Catal. Commun.*, 2009, **10**, 1486–1492.
8 J. J. Chiu, D. J. Pine, S. T. Bishop and B. F. Chmelka, *J. Catal.*, 2004, **221**, 400–412.
9 R. Luque, J. M. Campelo, D. Luna, J. M. Marinas and A. A. Romero, *Microporous Mesoporous Mater.*, 2005, **84**, 11–20.
10 S. Pega, C. Boissière, D. Grosso, T. Azaïs, A. Chaumonnot and C. Sanchez, *Angew. Chem., Int. Ed.*, 2009, **48**, 2784–2787.
11 D. Zhao, J. Feng, Q. Huo, N. Melosh, G. H. Fredrickson, B. F. Chmelka and G. D. Stucky, *Science*, 1998, **279**, 548–552.
12 Y. Zhao, C. Gao, Y. Li and T. Zhang, *Microporous Mesoporous Mater.*, 2009, **124**, 42–44.
13 J. M. Kim, S. Jun and R. Ryoo, *J. Phys. Chem. B*, 1999, **103**, 6200–6205.
14 C. L. Li, Y. Q. Wang, Y. L. Guo, X. H. Liu, Y. Guo, Z. G. Zhang, Y. S. Wang and G. Z. Lu, *Chem. Mater.*, 2007, **19**, 173–178.
15 D. Li, Y. Han, J. Song, L. Zhao, X. Xu, Y. Di and F. Xiao, *Chem.–Eur. J.*, 2004, **10**, 5911–5922.
16 D. Yang, Y. Xu, D. Wu and Y. Sun, *J. Solid State Chem.*, 2008, **181**, 2401–2405.
17 R. Mokaya, *Angew. Chem., Int. Ed.*, 1999, **38**, 2930–2934.
18 Q. H. Xia, K. Hidajat and S. Kawi, *Mater. Lett.*, 2000, **42**, 102–107.
19 G. D. Chen, L. Z. Wang, J. Y. Lei and J. L. Zhang, *Microporous Mesoporous Mater.*, 2009, **124**, 204–209.
20 A. K. Ghosh and R. A. Kydd, *Catal. Rev. Sci. Eng.*, 1985, **27**, 539–589.
21 R. B. Borade and A. Clearfield, *J. Chem. Soc., Faraday Trans.*, 1995, **91**, 539–547.
22 Y. Li, W. H. Zhang, L. Zhang, Q. H. Yang, Z. B. Wei, Z. C. Feng and C. Li, *J. Phys. Chem. B*, 2004, **108**, 9739–9744.
23 Y. Liu, W. Z. Zhang and T. J. Pinnavaia, *Angew. Chem., Int. Ed.*, 2001, **40**, 1255–1258.
24 Y. Han, S. Wu, Y. Y. Sun, D. S. Li, F. S. Xiao, J. Liu and X. Z. Zhang, *Chem. Mater.*, 2002, **14**, 1144–1148.
25 Q. F. Tan, X. J. Bao, T. C. Song, Y. Fan, G. Shi, B. J. Shen, C. H. Liu and X. H. Gao, *J. Catal.*, 2007, **251**, 69–79.
26 C. Song and Z. Yan, *Asia-Pac. J. Chem. Eng.*, 2008, **3**, 275–283.
27 M. Grun, I. Lauer and K. K. Unger, *Adv. Mater.*, 1997, **9**, 254–257.
28 S. Liu, P. Cool, O. Collart, P. Van Der Voort, E. F. Vansant, O. I. Lebedev, G. Van Tendeloo and M. Jiang, *J. Phys. Chem. B*, 2003, **107**, 10405–10411.
29 B. Tan and S. E. Rankin, *J. Phys. Chem. B*, 2004, **108**, 20122–20129.
30 B. Pauwels, G. V. Tendeloo, C. Thoelen, W. V. Rhijn and P. A. Jacobs, *Adv. Mater.*, 2001, **13**, 1317–1320.
31 Y. T. Yu, H. B. Qiu, X. W. Wu, H. C. Li, Y. S. Li, Y. Sakamoto, Y. Inoue, K. Sakamoto, O. Terasaki and S. N. Che, *Adv. Funct. Mater.*, 2008, **18**, 541–550.
32 J. G. Wang, F. Li, H. J. Zhou, P. C. Sun, D. T. Ding and T. H. Chen, *Chem. Mater.*, 2009, **21**, 612–620.
33 B. Tan, H. J. Lehmler, S. M. Vyas, B. L. Knutson and S. E. Rankin, *Chem. Mater.*, 2005, **17**, 916–925.
34 B. Tan and S. E. Rankin, *J. Phys. Chem. B*, 2004, **108**, 20122–20129.
35 J. G. Wang, Q. Xiao, H. J. Zhou, P. C. Sun, D. T. Ding and T. H. Chen, *J. Colloid Interface Sci.*, 2008, **323**, 332–337.
36 E. P. Parry, *J. Catal.*, 1963, **2**, 371–379.
37 K. Y. Wang, X. S. Wang and G. Li, *Microporous Mesoporous Mater.*, 2006, **94**, 325–329.
38 R. Le Van Mao, T. S. Le, M. Fairbairn, A. Muntasar, S. Xiao and G. Denes, *Appl. Catal., A*, 1999, **185**, 41–52.
39 M. C. Xu, W. Wang, M. Seiler, A. Buchholz and M. Hunger, *J. Phys. Chem. B*, 2002, **106**, 3202–3208.
40 C. Wang, Y. Du, D. Li, X. Guan, F. Li and F.-S. Xiao, *J. Colloid Interface Sci.*, 2008, **319**, 370–373.
41 G. Coudurier, C. Naccache and J. C. Vedrine, *J. Chem. Soc., Chem. Commun.*, 1982, 1413.
42 D. B. Shukla and V. P. Pandya, *J. Chem. Technol. Biotechnol.*, 1989, **44**, 147–154.
43 C. S. Blackwell, *J. Phys. Chem.*, 1979, **83**, 3251–3257.
44 H. H. P. Yiu and D. R. Brown, *Catal. Lett.*, 1998, **56**, 57–64.
45 M. J. Gracia, E. Losada, R. Luque, J. M. Campelo, D. Luna, J. M. Marinas and A. A. Romero, *Appl. Catal., A*, 2008, **349**, 148–155.

This journal is © The Royal Society of Chemistry 2011